Neuron

CellPress

Primer

Mesoscopic Imaging: Shining a Wide Light on Large-Scale Neural Dynamics

Jessica A. Cardin,[1] Michael C. Crair,[1] and Michael J. Higley[1,*]
[1]Department of Neuroscience, Kavli Institute for Neuroscience, Yale University School of Medicine, New Haven, CT 06510, USA
*Correspondence: m.higley@yale.edu
https://doi.org/10.1016/j.neuron.2020.09.031

SUMMARY

Optical imaging has revolutionized our ability to monitor brain activity, spanning spatial scales from synapses to cells to circuits. Here, we summarize the rapid development and application of mesoscopic imaging, a widefield fluorescence-based approach that balances high spatiotemporal resolution with extraordinarily large fields of view. By leveraging the continued expansion of fluorescent reporters for neuronal activity and novel strategies for indicator expression, mesoscopic analysis enables measurement and correlation of network dynamics with behavioral state and task performance. Moreover, the combination of widefield imaging with cellular resolution methods such as two-photon microscopy and electrophysiology is bridging boundaries between cellular and network analyses. Overall, mesoscopic imaging provides a powerful option in the optical toolbox for investigation of brain function.

INTRODUCTION

The use of various imaging modalities to monitor the electrical activity of neurons has provided essential insights into the workings of the nervous system. Early studies made use of autoradiography to map neuronal signaling indirectly by reading out metabolic activity (Thompson et al., 1983; Tootell et al., 1988). Activity-dependent changes in blood flow provide the basis for both intrinsic signal imaging and functional magnetic resonance imaging (Grinvald et al., 1986; Logothetis et al., 2001), techniques that have broadly shaped our understanding of brain function. More recently, the development of molecular probes that couple neuronal signals to fluorescence have revolutionized neuroscience, contributing to discoveries at the cellular and network levels (Lin and Schnitzer, 2016). Indeed, the impressive breadth of spatial and temporal scales over which neuronal activity is generated and organized remains an ongoing challenge to current research efforts. Single cells integrate thousands of synaptic inputs and are, in turn, connected into local microcircuits. These circuits are further organized into dynamic networks that may conceptually span the entire nervous system. In the mammalian neocortex, such large-scale networks are thought to provide the basis for cognition and complex behavior (Damoiseaux et al., 2006; Rubinov and Sporns, 2010; Stafford et al., 2014). A number of imaging strategies have emerged in recent decades for investigating distinct niches of spatiotemporal dynamics. However, there are limited methodologies that can provide high spatial and temporal resolution combined with the extremely large field of view necessary for answering questions about network function. In this Primer, we provide an overview of mesoscopic fluorescence imaging, a rapidly developing approach that directly addresses this challenge. We define mesoscopic imaging as a widefield, single-photon, fluorescence-based modality that can monitor activity across multiple millimeters of tissue at video frame rate. This approach enables recording from the entire dorsal neocortex in awake, behaving rodents. Here, we will summarize some of the central methods, highlight advantages and limitations, and discuss some recent biological discoveries that have emerged through this imaging modality.

MESOSCOPIC FLUORESCENCE IMAGING OF CORTICAL ACTIVITY

Fluorescent Imaging of Neuronal Calcium

Recent groundbreaking work from many laboratories has developed a number of distinct genetically encoded fluorescent indicators capable of reporting intracellular calcium (Ca^{2+}) (Chen et al., 2013; Dana et al., 2016), transmembrane voltage (Hochbaum et al., 2014; Villette et al., 2019), and extracellular transmitter molecules including glutamate, acetylcholine, and norepinephrine (Feng et al., 2019; Jing et al., 2018; Marvin et al., 2018). Most of these probes are fully compatible with widefield microscopy and will undoubtedly provide critical new insight into nervous system function. However, for the present Primer on mesoscopic imaging, we will primarily focus on fluorescent Ca^{2+} sensors as the most common exemplar of this growing field.

Fluorescence refers to the emission of photons by molecules that have previously absorbed light, typically of shorter wavelength. Excitation and emission spectra are highly dependent on the chemical properties of the individual fluorophore, a feature widely exploited in the development of fluorescent reporters for neuronal activity (Chen et al., 2013; Hochbaum et al., 2014; Jin et al., 2012; Lin and Schnitzer, 2016). In general, such indicators shift their sensitivity or spectral range as a function of their atomic conformation. For example, membrane-tethered sensors that undergo conformational shifts in response to changes in local electric fields can provide a readout of

transmembrane voltage. Many of the earliest studies using widefield imaging to monitor cortical function *in vivo* made use of voltage indicators, revealing spontaneous and sensory-evoked patterns of activity that spread over large regions (Ferezou et al., 2006, 2007; Mohajerani et al., 2010). Complementary to voltage sensing, a variety of engineered molecules shift their fluorescent properties upon binding ionic Ca^{2+}. As neuronal depolarization can drive the opening of voltage-gated Ca^{2+} channels, the large signal-to-noise afforded by many Ca^{2+} indicators has made them a critical, albeit indirect, sensor of activity at the cellular and network scale (Chen et al., 2013; Higley and Sabatini, 2008). Given the key role of Ca^{2+} indicators in many recent studies using mesoscopic imaging, we will discuss this class of probes in greater detail.

Indicators for intracellular Ca^{2+} are generally developed from either synthetic buffers (e.g., BAPTA) or calcium-binding proteins (e.g., calmodulin) that are covalently bonded to a suitable fluorophore (Brain and Bennett, 1997; Nakai et al., 2001; Tsien et al., 1996). For example, the widely used genetically encoded Ca^{2+} indicator (GECI) GCaMP is a fusion protein comprising calmodulin, the M13 myosin light-chain kinase sequence, and circularly permuted GFP (Chen et al., 2013; Nakai et al., 2001; Tian et al., 2009). GCaMP increases its excitation efficiency upon Ca^{2+} binding, resulting in increased green fluorescence during neuronal activity. Recent versions, including GCaMP6 and GCaMP7, provide incredibly bright, faithful reporting of intracellular Ca^{2+}, and specific variants exist that are "tuned" for variations in affinity, signal to noise, and decay kinetics (Chen et al., 2013; Dana et al., 2019). In addition, the emergence of red-shifted GECIs has expanded the chromatic palette and enabled simultaneous imaging of multiple cell types expressing different indicators (Dana et al., 2016). Nevertheless, there are some caveats associated with the application of Ca^{2+} sensors. Most notably, as buffers, these indicators sequester intracellular Ca^{2+} and prevent its interaction with endogenous partners. This buffering reduces peak Ca^{2+} concentration, prolongs temporal decay, and expands diffusional spread in response to transient activity (Higley and Sabatini, 2008). The potential consequences of these actions for cellular health and function will likely vary with indicator affinity, concentration, and cell type and must be considered when interpreting imaging data. For example, some (but not all) transgenic mouse lines expressing GCaMP6 are reported to exhibit aberrant cortical electrophysiology, including epileptiform activity (Daigle et al., 2018; Steinmetz et al., 2017), although the exact mechanisms underlying this pathology remain unclear.

Distinct Imaging Modalities for Probing Neuronal Signaling

As noted above, biochemical and electrical signaling by neurons spans multiple orders of magnitude in spatial and temporal scale, bridging molecular, cellular, systems, and behavioral subfields of neuroscience. A wide range of imaging modalities have been applied, in conjunction with fluorescent reporters, to investigate neural function. However, this methodological diversity means that finding the right match between tools and questions can be critical. Differences in imaging systems largely arise from variations in spatiotemporal resolution and invasiveness to the subject (see Box 1 for additional details). For example, two-photon microscopy provides cellular and subcellular resolution of neurons in awake, behaving mice. However, fields of view are typically restricted to a few hundred microns, and imaging requires a surgical opening through the skull for sufficient light penetration and imaging quality. Temporal resolution in most systems is limited to a few tens of frames per second due to the relatively slow rate of raster scanning across the sample, which may be insufficient to record fast events such as action potentials. Single-photon microscopy (including mesoscopic imaging) lacks the axial sectioning inherent to multiphoton modalities, and spatial resolution is highly limited by light scattering unless indicator expression is sparse. However, imaging can be performed (in some cases) through the intact skull, sampling rates can be very high (>1 kHz for some cameras), and fields of view can span several millimeters in diameter. Moreover, many scientific questions do not require cellular resolution (see below), and the relative simplicity of widefield imaging systems enables the implementation of head-mounted microscopes on freely moving mice (Rynes et al., 2020). In the following sections, we will provide an overview of mesoscopic imaging, a subclass of widefield, single-photon microscopy, that is currently experiencing rapid growth in neuroscientific applications.

Widefield "Mesoscopic" Imaging

Fluorescent Ca^{2+} imaging has been used to measure neuronal activity at a variety of spatial scales, ranging from single synapses, to local populations of individual neurons, to large-scale neuronal networks spanning multiple brain areas. Here, we focus on mesoscopic imaging, a widefield approach that has seen rapid development and implementation due to its relative ease of application and power to reveal novel aspects of neuronal network organization in behaving animals.

Mesoscopic imaging offers a powerful compromise between spatiotemporal resolution and field of view. Fluorescent signals are collected from the brain surface, either through a cranial window or intact skull, and image formation occurs via a microscope-coupled camera. Typical fields of view can span >100 mm^2 with a camera resolution of >512 × 512 pixels, resulting in single pixels corresponding to the spatially averaged activity of neurons located over a few tens of microns. Imaging is often performed at 10–50 frames per second, though higher rates are possible with newer cameras or pixel binning. Overall, this approach provides a readout of local circuit activity across the entire dorsal surface of the mouse neocortex with spatiotemporal resolution far surpassing other approaches with similar fields of view, such as intrinsic signal and functional magnetic resonance imaging (Grinvald et al., 1986; Schölvinck et al., 2010).

An additional advantage of mesoscopic imaging is the application of genetically encoded indicators, providing cell-type-specific expression and multi-color options for combined imaging of distinct cellular populations or signal types. For example, several transgenic mouse lines exist in which the Ca^{2+} indicator GCaMP6 is expressed pan-neuronally or under the control of the forebrain-specific excitatory promoter Thy1 (Dana et al., 2014; Madisen et al., 2015). In addition, transgenic mice harboring a conditional allele for GCaMP6 (Daigle et al., 2018; Madisen et al., 2012) can be crossed to lines in which Cre recombinase

Box 1.

Neural activity comprises both electrical and biochemical signals that can be monitored using a variety of optical approaches that differ in their ability to resolve spatial and temporal components. Advantages and disadvantages of each method must be weighed against specific experimental goals. Here, we briefly summarize several approaches with complementary benefits and limitations. We also identify a non-comprehensive list of representative studies to illustrate the different strategies, and additional references are found in the main text.

Widefield Fluorescence Imaging

Widefield imaging refers to a modality in which the entire sample is exposed to excitation light. Signals are typically collected and images formed via a camera (i.e., CCD or sCMOS). Temporal resolution is limited by the kinetics of the indicators and the camera frame rate, which can span a few frames per second to >1 kHz. Spatial resolution is limited by the microscope optics and pixel density of the camera. Many studies using small (<1 mm^2) fields of view have resolved individual neurons, collecting signals through an objective placed above the tissue or via an inserted lens. This modality has also given rise to head-mounted systems for monitoring brain activity in freely moving animals. Given the inherent lack of optical z-sectioning with widefield illumination, assigning emitted photons to a single imaging plane (versus multiple cells in close vertical register) can be a limitation. Mesoscopic widefield imaging, which trades spatial resolution for much larger fields of view (>100 mm^2), is a complementary approach. Thus, single cells are not resolved, but activity across wide areas (e.g., the entire dorsal cortical surface) can be imaged simultaneously at high frame rates. Selected references: Ackman et al. (2012); Aharoni et al. (2019); Barson et al. (2020); Kim et al. (2016); Kingsbury et al. (2019); Musall et al. (2019); Senarathna et al. (2019); Skocek et al. (2018); Vanni et al. (2017).

Multiphoton Fluorescence Imaging

Multiphoton imaging (including two- and three-photon variants) relies on exciting molecules with focused, high-intensity light that results in absorption of multiple infrared photons, followed by emission in standard visible ranges. The focused spot is scanned across the sample, and signals are collected via photomultiplier tubes. Images are formed post hoc by alignment of the collected signal with the known location of the focal position. Scanning is typically performed with galvanometric mirrors, and frame rates are limited in most cases to <100 Hz. These systems rely on high numerical aperture objectives that are usually limited to small fields of view (<1 mm^2). However, spatial resolution is high (<1 μm), providing excellent imaging of cellular and subcellular structures. Moreover, multiphoton imaging provides inherent optical z-sectioning as only molecules near the focal plane are excited. Recent developments have increased the functional field of view by use of multi-beam scanning or translating the imaging window across different positions. Multiphoton imaging systems typically much more expensive than their widefield counterparts due to the necessity for complex microscopes and laser light sources. Selected references: Barson et al. (2020); Denk and Svoboda (1997); Smith et al. (2013); Sofroniew et al. (2016); Stirman et al. (2016); Wang et al. (2020b); Xu et al. (2012).

Fiber Photometry

A relatively new approach in fluorescence-based monitoring of neuronal activity, fiber photometry relies on exciting the sample and collecting emitted photons through a fiber optic that can be implanted anywhere in the brain. Temporal resolution is essentially unlimited, while there is no spatial resolution as all photons emitted from the target region are integrated into a single channel in the fiber. Multiple wavelengths can be combined in the same fiber for imaging different cellular populations. Thus, photometry can provide a relatively inexpensive yet powerful tool for monitoring neural activity in deep brain structures and is also readily combined with other imaging and electrophysiology modalities. Selected references: Gunaydin et al. (2014); Meng et al. (2018); Pisano et al. (2019).

is selectively expressed in distinct cell types, including diverse classes of excitatory and inhibitory populations (Hippenmeyer et al., 2005; Taniguchi et al., 2011). The use of viral vectors, such as adeno-associated virus (AAV), has further broadened the ability to target indicator expression to specific brain regions or cell types. AAVs can drive robust expression of GCaMP6 in cell bodies, dendrites, and axons within days to weeks, following either local or systemic injection (Barson et al., 2020; Chan et al., 2017; Chen et al., 2013; Hamodi et al., 2020). AAV-driven expression can also take advantage of recombinase-mediated cell-type specificity, and targeting can be also enhanced by variation in viral serotype or transcriptional regulators (Deverman et al., 2016; Dimidschstein et al., 2016; Tervo et al., 2016). Finally, intersectional viral strategies can be used to label projection-specific subclasses of cells, using retrograde AAV-driven expression of Cre recombinase and anterograde AAV-driven expression of a Cre-dependent GCaMP6 (Tang and Higley, 2020; Tervo et al., 2016).

Both commercial and custom-built imaging systems have been used successfully for mesoscopic imaging. Indeed, the relatively low cost of necessary hardware is a major advantage of mesoscopic versus other modalities, such as multiphoton imaging. A low-magnification objective with a large field of view and high sensitivity camera are the most essential elements (see next section). While large fields of view encompassing the entire cortical mantle generally require a head-fixed animal placed under a stable microscope, ongoing development of small systems are pushing the limits of mesoscopic imaging in freely moving mice (Rynes et al., 2020). In the following section, we will provide an in-depth discussion of approaches for collecting and analyzing mesoscopic signals from the mouse neocortex.

ACQUISITION AND ANALYSIS OF MESOSCOPIC DATA

We will now outline a general experimental strategy for mesoscopic imaging used successfully by our groups and similar to

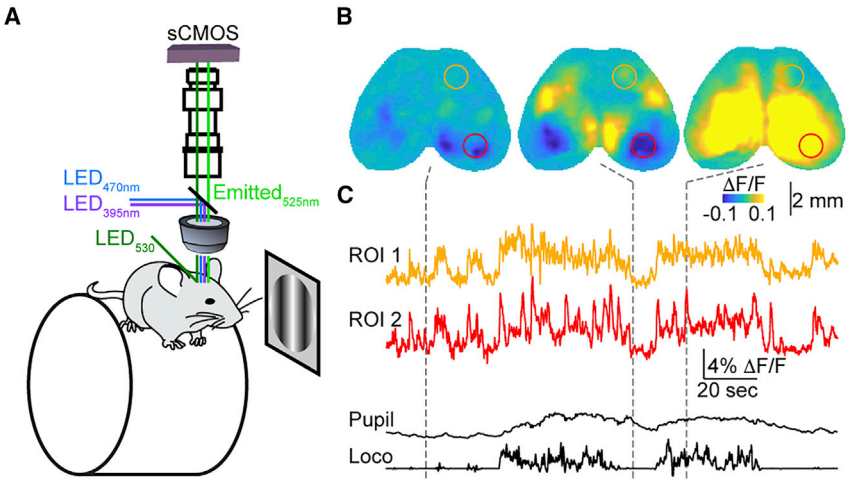

Figure 1. Mesoscopic Imaging of Neural Activity in the Mouse Neocortex

(A) Schematic illustrating the imaging system for acquiring mesoscopic fluorescence imaging data in the mouse. Ca^{2+} indicators are excited via output from an LED engine (violet and blue), and emitted (green) photons are collected through a large field-of-view objective and imaged via sCMOS camera. Reflected green light from a separate LED source can also be used to measure hemodynamic signals. The mouse is positioned on a running wheel for monitoring behavioral state, and a nearby display can deliver visual stimulation.

(B) Example mesoscopic imaging frames showing time-varying and spatially heterogeneous signals in the awake mouse.

(C) Time series of activity corresponding to the indicated regions of interest (ROI) indicated by circles in (B). Dashed lines indicate time of frames shown in (B). Bottom traces indicate simultaneously monitored pupil diameter and locomotion (wheel speed).

systems from other laboratories (Barson et al., 2020; Clancy et al., 2019; Musall et al., 2019). We will also discuss some of the component options that may vary across setups from different groups. We emphasize that the ease of modifying or adapting the approach to the individual needs of each experiment is one of the powerful aspects of this imaging strategy (Figure 1).

Mesoscopic imaging is generally carried out using mice broadly expressing indicator throughout the neocortex. This may include transgenic lines (e.g., Thy1-GCaMP6s, tetO-GCaMP6, or Vglut1-Cre;Ai162) (Daigle et al., 2018; Dana et al., 2014; Wekselblatt et al., 2016) or mice injected intravascularly at birth with serotype 9 AAV, which we showed results in widespread expression (Barson et al., 2020; Hamodi et al., 2020). Notably, we have also found that GCaMP6 expression restricted to small cell populations (such as vasoactive intestinal peptide-expressing interneurons, ~2%–3% of all cortical cells) still produces a robust transcranial signal. Prior to imaging (~1–2 weeks), the subject is surgically implanted with a light-weight titanium head post and the scalp is retracted. The skull surface can be cleaned, coated in cyanoacrylate or clear dental cement, and polished to reduce light scattering, with several groups either thinning the skull or cementing a cover glass over the exposed bone (Cramer et al., 2019; Kozberg et al., 2016; Silasi et al., 2016; Valley et al., 2020; Vanni et al., 2017). We and others have successfully carried out mesoscopic imaging through the intact skull of mice as old as 1 year of age (Aruljothi et al., 2020; Barson et al., 2020; Clancy et al., 2019; Cramer et al., 2019; Gilad and Helmchen, 2020; MacDowell and Buschman, 2020; Musall et al., 2019; Peters et al., 2019; Shimaoka et al., 2019; Valley et al., 2020; Vanni et al., 2017). However, other groups have performed similar studies after replacing the skull with a transparent window (Allen et al., 2017; Liu et al., 2019; Rynes et al., 2020; Scott et al., 2018; Sit and Goard, 2020; Wekselblatt et al., 2016; Xiao et al., 2017), which increases optical access but raises the possibility of inflammation or damage that can alter normal cortical activity. Indeed, a direct comparison of transcranial versus implanted window preparations is lacking and represents a topic for further exploration by the field. For our experiments, mice are head-fixed above a freely rotating wheel, and behavioral state is constantly monitored using wheel speed (locomotion) as well as whisking and pupil diameter recorded with a small camera placed near the animal (Barson et al., 2020; Tang and Higley, 2020; Vinck et al., 2015).

The microscope setup can vary substantially between laboratories, although the essential components include an excitation light source, an optical relay system, and a camera for image formation. Fluorophore excitation is typically provided by a light-emitting diode (LED) engine, often strobing different wavelengths on alternating frames to excite multiple chromatically distinct indicators or correct for activity-independent signal contamination. For example, GCaMP6 exhibits isosbestic excitation (equivalent absorption for Ca^{2+}-bound and -unbound forms) at violet (~400 nm) wavelengths, providing a potential method for correcting green fluorescence signals due to motion or hemodynamic artifacts (Allen et al., 2017; Barson et al., 2020; Tian et al., 2009) (see Limitations below for additional details on hemodynamic artifacts). Custom-built microscopes often incorporate an inverted, tandem lens system that provides a low (<1.5×) magnification and large field of view (Cramer et al., 2019; Gilad and Helmchen, 2020; MacDowell and Buschman, 2020; Musall et al., 2019; Peters et al., 2019; Scott et al., 2018; Valley et al., 2020; Vanni et al., 2017; Wekselblatt et al., 2016; Zatka-Haas et al., 2019). Alternatively, several commercial options (e.g., Zeiss, RedShirt Imaging, Olympus) provide mesoscopic systems with added features and technical support, though at a higher cost (Ackman et al., 2012; Aruljothi et al., 2020; Barson et al., 2020; Gribizis et al., 2019; Matsui et al., 2016). Virtually all recent studies collect emitted signals for image formation using scientific CMOS cameras, which provide sufficient sensitivity with large sensor sizes, high pixel densities, and very fast (up to 1,000 frames per second in some cases) acquisition rates. Many modern cameras are capable of acquiring images at >4 megapixels. However, most groups use binning, either on camera or in post hoc processing, to reduce final images to 512 × 512 pixels or less, increasing frame rates and reducing file sizes. Indeed, 512 × 512 images, recorded at 12-bit depth and 30 frames per second, produce ~100 Mbs data, requiring sufficient

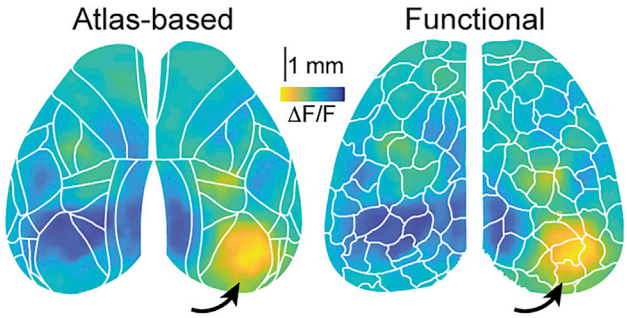

Figure 2. Diverse Strategies for Parcellation of Cortical Regions for Imaging Analysis

Two examples for parcellating (segmenting) mesoscopic imaging data collected from a single mouse, showing the averaged response to a visual stimulus (arrow). Using a standard atlas based on averaged anatomical and molecular datasets, such as the Allen Institute CCFv3 (left) (Wang et al., 2020a), allows straightforward alignment and grouped analysis for multiple individual animals. A contrasting approach uses correlational analyses of activity to group pixels into parcels that may be unique for a given individual (right) (Mishne et al., 2018). Both methods can yield similar numbers of parcels but often with markedly different boundaries.

computer memory and fast solid-state hard drives to avoid dropping frames during acquisition. Depending on the field of view, these parameters result in a single pixel representing ~100–10,000 μm^2 of cortical area.

Mesoscopic data analysis generally follows a three-stage procedure that includes pre-processing, parcellation, and quantification. As with acquisition systems, this approach is easily modified or expanded. Pre-processing often includes detrending, noise reduction, and correction for signal contamination. Many fluorescent reporters exhibit bleaching that produces a slow change in both baseline and transient signal amplitude. This time-dependent loss of fluorescence can be addressed by low-pass filtering of the signal, followed by subtraction and normalization of the original data by this "baseline" F_0, resulting in standard $\Delta F/F_0$ values. Normalization by F_0 also corrects for variation in optical path length, indicator expression levels, excitation intensity, and detector sensitivity, allowing for more robust comparisons across microscopes and studies. Electronic and photonic shot noise can be reduced by a combination of additional filtering and pixel binning. Imaging artifacts (e.g., hemodynamic absorption) can be more challenging to address and typically require estimating the contaminating signal and correction of the raw data (see Limitations below) (Barson et al., 2020; Ma et al., 2016a; Tian et al., 2009).

Following pre-processing, the high dimensionality of the raw data is typically reduced by grouping pixels together into common regions or parcels (Figure 2). Methods for parcellation are actively being developed by many groups, although a common approach is to use an anatomical reference atlas such as the Allen Institute CCFv3 (Wang et al., 2020a). For this strategy, the cortex is segmented into common subregions based on projection patterns and molecular markers, and pixels are assigned to a particular subregion based on gross alignment of the individual brain to the reference atlas (Barson et al., 2020; Musall et al., 2019; Saxena et al., 2020). This approach has the advantage of standardizing measurements across individual animals and research groups. However, the accuracy of atlas-based parcellation for individual animals is unclear, and aligning individual brains to a reference can be difficult. Such alignment may be made easier by registering surface blood vessels to post hoc serial reconstructions (Orsolic et al., 2019). An alternative approach is to use functional measures, such as spatiotemporal correlations in activity between pixels, to formulate a parcellation that can vary from animal to animal (Barson et al., 2020; Lake et al., 2018; Mishne et al., 2018). This strategy has the advantage of reflecting underlying activity for the individual, but the number and borders of functionally defined parcels may vary across animals (or even across sessions within animal), raising challenges for statistical analyses and interpretation. Hybrid approaches are also possible, where activity is used to refine segmentation seeded by a reference atlas (Saxena et al., 2020). Similarly, mesoscopic imaging can be used to identify borders of retinotopically defined visual areas, whose specific boundaries may vary across individuals but are categorically conserved (Sit and Goard, 2020). Finally, a recent study defined spatiotemporal motifs that reflected repeated patterns of activation in potentially overlapping cortical areas (MacDowell and Buschman, 2020). Perhaps most importantly, within-subject comparisons of functional parcellations with complementary labeling strategies using molecular or anatomical markers (Daigle et al., 2018; Wang et al., 2020a) are lacking and would represent a critical step forward.

Quantification of mesoscopic data after pre-processing and parcellation is clearly the most diverse and open-ended element of analysis, and the specific approach employed will vary depending on the nature of the scientific question under study. The relative ease of this imaging modality allows investigators to relate mesoscopic signals to behavioral-state variables (Barson et al., 2020; Clancy et al., 2019), task acquisition and performance (Musall et al., 2019; Orsolic et al., 2019; Wekselblatt et al., 2016), sensory maps (Sit and Goard, 2020), and the development of neural circuits (Burbridge et al., 2014; Gribizis et al., 2019). We will summarize a number of recent biological findings made possible through mesoscopic imaging in the subsequent sections.

LIMITATIONS OF MESOSCOPIC IMAGING

Despite the power of mesoscopic Ca^{2+} imaging to drive novel insights into network organization and function (see below), there are a number of limitations to this modality that must be considered. As noted above, strong expression of genetically encoded indicators, particularly during early brain development, may contribute to pathological activity in the brain (Daigle et al., 2018; Steinmetz et al., 2017). Also, camera pixel resolution is approximately tens of microns, and light scattering through brain and skull tissue further reduce the functional resolution, thereby preventing data on single-cell activity. Moreover, most current methods for expressing Ca^{2+} indicators in neurons give rise to fluorescent signals in cell bodies, dendrites, and axons, creating a summed signal that reflects activity in somata and neuropil (Barson et al., 2020; Chen et al., 2013; Harris et al., 2016; Peron et al., 2015). While somatic Ca^{2+} imaging is assumed to report action-potential-driven current through voltage-gated calcium channels, mesoscopic Ca^{2+} signals may also arise from dendritic

calcium channels, including glutamate receptors (Higley and Sabatini, 2008). Finally, the fluorescence signal recorded from the cortical surface represents a weighted mix of signals by depth, heavily biased toward superficial layers (Ma et al., 2016a). This heterogeneity raises substantial challenges for post hoc interpretation of the underlying neural activity. For example, many strategies attempt to derive single-cell spike rates from two-photon somatic Ca^{2+} imaging using deconvolution of the data with a temporal kernel representing the relationship between a single action potential and the resulting fluorescence signal (Pachitariu et al., 2018; Vogelstein et al., 2010). Given the lack of a single kernel for mesoscopic data, similar efforts may be difficult for this modality (Stern et al., 2020). Nevertheless, one potential solution to this issue is expression targeted to specific cellular compartments (e.g., soma- or axon-restricted expression). Ca^{2+} indicators can be restricted to the nucleus via nuclear localization sequences (Bengtson et al., 2010; Kim et al., 2014), but this may slow the temporal resolution of the reporter due to the requirement for Ca^{2+} passage across the nuclear membrane. New soma-targeted GCaMP variants may provide a different approach by restricting GCaMP to the cell body via fusion to ribosomes or other proteins (Chen et al., 2020; Shemesh et al., 2020). Finally, despite the limited determinacy of signal origin, the functional resolution of mesoscopic imaging is fully sufficient to address many essential questions in neuroscience, as compared to other approaches. For example, the spatial resolution of local field potentials, which largely represent synaptic activity, is approximately 200–400 μm or more (Buzsáki et al., 2012), while the resolution of fMRI is typically >500 μm (Shmuel et al., 2007). In this light, mesoscopic Ca^{2+} signals are best conceptualized as a reporter of local circuit dynamics.

A second limitation for analysis of mesoscopic data is the potential contamination of optical signals by activity-dependent changes in local blood volume and oxygenation. Indeed, fluctuations in diffuse optical reflectance without application of exogenous indicators are termed "intrinsic signals," and imaging this activity became a standard approach for mapping functional areas in the cortex (Chen et al., 2005; Das and Gilbert, 1997; Malonek and Grinvald, 1996). Hemoglobin broadly absorbs photons over the visible range, varying with its oxygenation state (Ma et al., 2016a). For fluorescence imaging, this implies that fluctuations in both total blood flow and blood oxygenation will alter excitation and emission photons related to fluorescence imaging, leading to possible confounds in signal interpretation. Notably, this confound is not resolved simply by using brighter indicators, as the consequences of hemodynamic absorption will scale with the emitted signal (Ma et al., 2016a). Given the strong correlation of cortical blood flow and neural activity (Logothetis et al., 2001; Malonek and Grinvald, 1996), the potential contamination of fluorescence data by hemodynamic absorption requires careful consideration.

Two general approaches have been used to correct for hemodynamic contamination. The first method makes use of the isosbestic excitation of GCaMP6 at violet (~400 nm) versus standard blue (~488 nm) wavelengths. Green fluorescence under these conditions is independent from calcium binding, meaning that fluctuations in emitted photons can be attributed to other processes (e.g., hemodynamic or movement artifacts). By rapidly alternating imaging frames between the two different excitation wavelengths, the violet-excited signal can be used to remove these contaminants from the blue-excited Ca^{2+}-dependent signal using regression (Allen et al., 2017; Barson et al., 2020; Tian et al., 2009). One caveat to this approach is that it fails to account for differential absorption of violet versus blue excitation light by hemoglobin, essentially only correcting for confounds of the emission signal. In addition, hemodynamic absorption is multiplicative with indicator fluorescence, limiting the utility of basic regression-based linear corrections. A second method relies on the direct measurement of hemodynamic absorption based on reflectance of green and red photons that are differentially absorbed by oxygenated and deoxygenated hemoglobin (Ma et al., 2016a; Valley et al., 2020). In this case, alternating frames between blue (~488 nm), green (~530 nm), and red (~630 nm) exposure provides emitted/reflected signals corresponding to uncorrected Ca^{2+}-dependent fluorescence, total hemoglobin (due to isosbestic green absorption), and reduced hemoglobin. These signals can be used to formulate a more accurate correction factor for hemodynamic absorption (Kozberg et al., 2016; Ma et al., 2016a). Moreover, estimating hemodynamics with these approaches provides a complementary measure of physiological activity collected simultaneously with fluorescence signals linked to neuronal firing. Neurovascular coupling is an important aspect of brain function and represents the foundation of functional magnetic resonance imaging (Logothetis et al., 2001; Ma et al., 2016b).

Importantly, the practical consequences of signal contamination by changes in blood flow and oxygenation are not well documented across the field, representing a major need for continued study. For example, variation in surgical preparation (e.g., intact or removed skull), spatial heterogeneity of indicator expression across the cortical thickness, and variations in indicator spectra (e.g., green versus red fluorescence) will all increase the complexity of interpreting results. Furthermore, there is minimal "ground truth" data establishing the magnitude of the confound under different experimental conditions or whether the different correction methods yield qualitatively or quantitatively different results. Finally, the potentially variable coupling of neuronal activity to hemodynamic fluctuations for different temporal scales or cell types is not well understood. While many recent studies have employed specific correction strategies (Allen et al., 2017; Barson et al., 2020; Kozberg et al., 2016), others have omitted any correction for hemodynamic artifacts (Aruljothi et al., 2020; Gilad and Helmchen, 2020; Liu et al., 2019; Sit and Goard, 2020) or suggested that correction provided only modest impact on final analyses (MacDowell and Buschman, 2020), again emphasizing the need for additional investigation.

Finally, mesoscopic imaging has generally been limited to the brain areas accessible from the surface (e.g., dorsal neocortex or superior colliculus) due to the requirement for large fields of view and corresponding optics. Thus, direct access to most subcortical structures is lacking. However, mesoscopic imaging can be paired with extracellular recordings (Clancy et al., 2019; Xiao et al., 2017; Zatka-Haas et al., 2019) to provide simultaneous access to cortical networks and single- or multi-unit recordings of activity in targeted subcortical areas. Mesoscopic imaging of axonal terminals (e.g., retinotectal or thalamocortical)

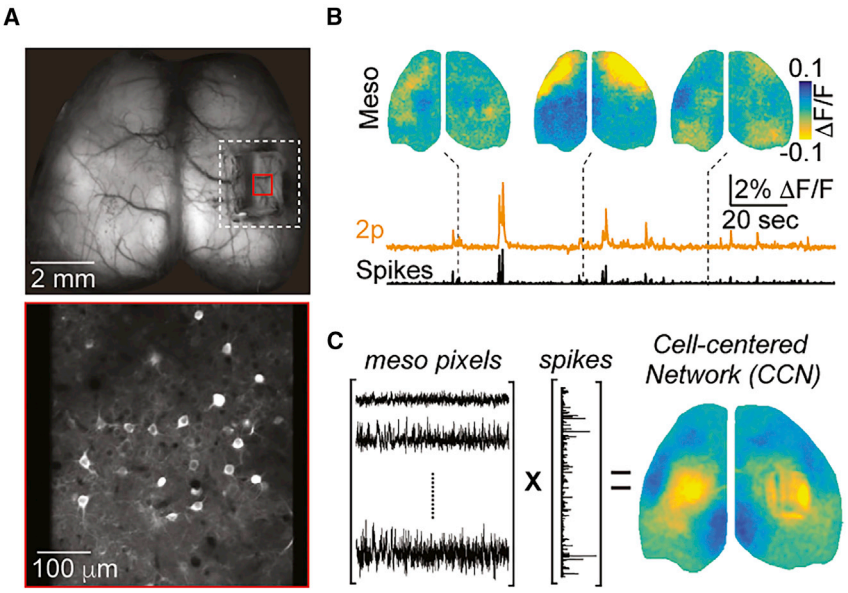

Figure 3. Example Showing Analysis of Functional Connectivity in Cortical Networks Determined by Dual Two-Photon and Mesoscopic Imaging

(A) Example image frames showing raw mesoscopic (upper) and two-photon (lower) fields of view. The two-photon data were collected through a microprism implanted on the cortical surface, highlighted by the white dashed box. The inner red box highlights the two-photon field of view.

(B) Example traces showing three mesoscopic imaging frames aligned with the two-photon imaged activity of a single neuron (orange) and the inferred neuronal spike data (black).

(C) Schematic showing the calculation of cell-centered networks (CCNs) using the dot product of neuronal spike data and each mesoscopic pixel. Each CCN represents the functional connectivity of a single neuron to the large-scale cortical network. Adapted from Barson et al. (2020).

is also possible and can provide additional access to neurons whose cell bodies are not visible from the surface (Ackman et al., 2012; Gribizis et al., 2019). Finally, combining mesoscopic imaging with fiber photometry in subcortical structures is also likely to be successful.

RECENT BIOLOGICAL INSIGHTS FROM MESOSCOPIC ANALYSIS

Many recent studies have highlighted the unique insights gained from performing mesoscopic imaging either alone or in combination with electrophysiology or other imaging modalities. For example, mesoscopic Ca^{2+} signals have been used to characterize the spatiotemporal dynamics of patterned cortical activity during early development and in the mature animal. Before eye opening, spontaneous waves in the retina shape the refinement of retinotopic maps in the developing cortex and superior colliculus (Ackman et al., 2012; Burbridge et al., 2014; Gribizis et al., 2019), whereas cortically generated activity may instruct the formation of long-range connectivity and sensory tuning (Smith et al., 2018). In adults, mesoscopic imaging can also identify patterns of spontaneous activity that may reflect a functionally connected resting-state network (Matsui et al., 2016; Vanni et al., 2017; Wright et al., 2017). Recent work has extended these findings and identified core spatiotemporal motifs of cortical activity that are generalized across animals and associated with specific sensory and behavioral contexts (MacDowell and Buschman, 2020; Wekselblatt et al., 2016). These patterned fluctuations in cortical activity can regulate sensory encoding and be coordinated across hemispheres, a scale too large to be observed by other imaging modalities (Shimaoka et al., 2019). Finally, mesoscopic Ca^{2+} imaging provides a high-resolution approach for identifying retinotopically organized primary and secondary areas of the visual cortex (Sit and Goard, 2020).

In addition to revealing patterned network activity in the healthy brain, mesoscopic imaging is well suited to identifying the origination and spread of pathological activity across interconnected cortical areas. Focal cortical seizures initiate as standing waves that can propagate according to this pattern of inter-areal functional connectivity (Montgomery et al., 2020; Rossi et al., 2017). Furthermore, connectivity between cortical areas can be restructured by pathological events such as stroke (Cramer et al., 2019). Finally, many neurodevelopmental disorders, including autism and schizophrenia, are hypothesized to result from perturbation of large-scale cortical networks (Worbe, 2015). Mesoscopic imaging of activity in mouse models of these conditions will likely drive critical new insights into links between genetic mutations, network dynamics, and behavior.

Mesoscopic imaging also presents a powerful approach for identifying functional connectivity of cortical networks across divergent spatial scales though a combination with cellular resolution methods. For example, recent work combining mesoscopic and two-photon Ca^{2+} imaging revealed the organization of single somatosensory cortex neurons with large-scale cortical networks. These cell-centered networks (CCNs) demonstrated considerable heterogeneity in the broad connectivity of neighboring neurons (Barson et al., 2020) (Figure 3). Indeed, multi-color imaging of genetically targeted cell types revealed additional diversity between excitatory and inhibitory populations. The structure of these CCNs can also be modulated by changes in behavioral state, a result also supported by a complementary strategy combining mesoscopic imaging with electrophysiological recordings of single units (Barson et al., 2020; Clancy et al., 2019). A similar combination of mesoscopic imaging with subcortical electrophysiology has further revealed differences in the motifs of neural activity associated with the spiking of thalamic and cortical neurons (Xiao et al., 2017).

Finally, mesoscopic imaging during performance of learned behaviors has revealed widespread representation of task-

related and -unrelated motor signals throughout the neocortex (Musall et al., 2019; Orsolic et al., 2019), a finding that raises intriguing questions about shared behavioral representations across distinct cortical areas. While widespread patterned activity is observed in correlation with learned behavior, only a small subset of active areas may be critical for task performance (Gilad and Helmchen, 2020; Zatka-Haas et al., 2019). However, broad cortical activation may play an important role in task-relevant subcortical activity in structures such as the basal ganglia (Peters et al., 2019). Interestingly, task-relevant cortical areas may be more easily identified when controlling for animal movement in the design of the task (Orsolic et al., 2019).

FUTURE ADVANCES

The utility and success of mesoscopic imaging is likely to benefit significantly from ongoing technical innovations across a range of avenues, further increasing our ability to probe the biological basis of behavior. For example, the development of brighter and more sensitive detectors will enhance both imaging quality and the diversity of behavioral paradigms available to investigators. Miniaturized head-mounted imaging systems have typically been limited to small fields of view, although recent work has demonstrated the potential for whole-cortex imaging in freely moving mice (Rynes et al., 2020). The combination of mesoscopic imaging with complex behavioral analyses, including social interaction and home-cage monitoring (Kingsbury et al., 2019; Puścian et al., 2016), will open new vistas into understanding brain function.

Another critical area of development is the generation of novel reporters for neuronal activity. Red fluorescing Ca^{2+} indicators provide orthogonal wavelengths for simultaneous imaging of multiple populations (Dana et al., 2016; Gribizis et al., 2019; Inoue et al., 2015). In addition, genetically encoded reporters for fast transmitters such as glutamate and GABA (Marvin et al., 2013, 2018, 2019) and neuromodulators such as norepinephrine, acetylcholine, and dopamine (Feng et al., 2019; Jing et al., 2018; Patriarchi et al., 2018; Sun et al., 2018) have been described that are compatible with mesoscopic imaging. Finally, the continued refinement of genetically encoded voltage sensors increases the utility of these probes for mesoscopic imaging at even faster temporal scales than currently accessible (Hochbaum et al., 2014; Jin et al., 2012; Villette et al., 2019).

A great benefit of genetically encoded indicators lies in the ability to target their expression to specific neuronal subpopulations. As noted, conditional labeling via Cre-recombinase-dependent expression (Madisen et al., 2012, 2015; Taniguchi et al., 2011) can enable mesoscopic imaging of distinct cortical cell types, for example, simultaneously monitoring large-scale network organization of excitatory and inhibitory cells. Ongoing development of mouse lines with greater specificity for unique subpopulations will further drive such studies. In addition, targeting soma-restricted fluorophores (to eliminate ambiguous neuropil signals) to specific cortical layers may overcome the lack of depth discrimination inherent to widefield imaging (Chen et al., 2020; Shemesh et al., 2020). Similarly, the development of novel viral strategies to label targeted subpopulations based on projection targets (Tang and Higley, 2020; Tervo et al., 2016) or cell-type-specific promoters (Dimidschstein et al., 2016; Jüttner et al., 2019; Vormstein-Schneider et al., 2020) will further expand the reach of mesoscopic analysis. Moreover, the ability of systemic AAV injection to drive widespread indicator expression offers the possibility of generalizing mesoscopic imaging to other species, including rats and other mammals (Barson et al., 2020; Chan et al., 2017; Hamodi et al., 2020; Scott et al., 2018).

Finally, as noted above, the combination of mesoscopic imaging with other measures of neural activity such as two-photon microscopy and electrophysiology can significantly accelerate the discovery of principles underlying brain function and connectivity at a range of spatiotemporal scales (Barson et al., 2020; Clancy et al., 2019; Peters et al., 2019). Similarly, mesoscopic imaging performed with simultaneous functional MRI allows measurement of activity throughout the depth of the brain and facilitates a better understanding of the cellular and circuit origins of blood-oxygen-level-dependent signals measured in both human and non-human studies (Lake et al., 2018).

ACKNOWLEDGMENTS

The authors are thankful to members of the Cardin, Crair, and Higley laboratories for their outstanding contributions to the development and application of imaging strategies described here and for helpful comments in the preparation of this review. This work was supported by funding from the NIH (R01 MH099045 and R21 MH121841 to M.J.H.; R01 MH113852 to M.J.H. and J.A.C.; R01 EY015788, R01 MH111424, and U01 NS094358 to M.C.C.; and P30 EY026878 to the Yale Vision Core), a Simons SFARI research grant to M.J.H. and J.A.C.; and a Ludwig Foundation grant to J.A.C.

REFERENCES

Ackman, J.B., Burbridge, T.J., and Crair, M.C. (2012). Retinal waves coordinate patterned activity throughout the developing visual system. Nature *490*, 219–225.

Aharoni, D., Khakh, B.S., Silva, A.J., and Golshani, P. (2019). All the light that we can see: a new era in miniaturized microscopy. Nat. Methods *16*, 11–13.

Allen, W.E., Kauvar, I.V., Chen, M.Z., Richman, E.B., Yang, S.J., Chan, K., Gradinaru, V., Deverman, B.E., Luo, L., and Deisseroth, K. (2017). Global Representations of Goal-Directed Behavior in Distinct Cell Types of Mouse Neocortex. Neuron *94*, 891–907.e6.

Aruljothi, K., Marrero, K., Zhang, Z., Zareian, B., and Zagha, E. (2020). Functional Localization of an Attenuating Filter within Cortex for a Selective Detection Task in Mice. J. Neurosci. *40*, 5443–5454.

Barson, D., Hamodi, A.S., Shen, X., Lur, G., Constable, R.T., Cardin, J.A., Crair, M.C., and Higley, M.J. (2020). Simultaneous mesoscopic and two-photon imaging of neuronal activity in cortical circuits. Nat. Methods *17*, 107–113.

Bengtson, C.P., Freitag, H.E., Weislogel, J.M., and Bading, H. (2010). Nuclear calcium sensors reveal that repetition of trains of synaptic stimuli boosts nuclear calcium signaling in CA1 pyramidal neurons. Biophys. J. *99*, 4066–4077.

Brain, K.L., and Bennett, M.R. (1997). Calcium in sympathetic varicosities of mouse vas deferens during facilitation, augmentation and autoinhibition. J. Physiol. *502*, 521–536.

Burbridge, T.J., Xu, H.P., Ackman, J.B., Ge, X., Zhang, Y., Ye, M.J., Zhou, Z.J., Xu, J., Contractor, A., and Crair, M.C. (2014). Visual circuit development requires patterned activity mediated by retinal acetylcholine receptors. Neuron *84*, 1049–1064.

Buzsáki, G., Anastassiou, C.A., and Koch, C. (2012). The origin of extracellular fields and currents–EEG, ECoG, LFP and spikes. Nat. Rev. Neurosci. *13*, 407–420.

Chan, K.Y., Jang, M.J., Yoo, B.B., Greenbaum, A., Ravi, N., Wu, W.L., Sánchez-Guardado, L., Lois, C., Mazmanian, S.K., Deverman, B.E., and

Gradinaru, V. (2017). Engineered AAVs for efficient noninvasive gene delivery to the central and peripheral nervous systems. Nat. Neurosci. *20*, 1172–1179.

Chen, L.M., Friedman, R.M., and Roe, A.W. (2005). Optical imaging of SI topography in anesthetized and awake squirrel monkeys. J. Neurosci. *25*, 7648–7659.

Chen, T.W., Wardill, T.J., Sun, Y., Pulver, S.R., Renninger, S.L., Baohan, A., Schreiter, E.R., Kerr, R.A., Orger, M.B., Jayaraman, V., et al. (2013). Ultrasensitive fluorescent proteins for imaging neuronal activity. Nature *499*, 295–300.

Chen, Y., Jang, H., Spratt, P.W.E., Kosar, S., Taylor, D.E., Essner, R.A., Bai, L., Leib, D.E., Kuo, T.W., Lin, Y.C., et al. (2020). Soma-Targeted Imaging of Neural Circuits by Ribosome Tethering. Neuron *107*, 454–469.e6.

Clancy, K.B., Orsolic, I., and Mrsic-Flogel, T.D. (2019). Locomotion-dependent remapping of distributed cortical networks. Nat. Neurosci. *22*, 778–786.

Cramer, J.V., Gesierich, B., Roth, S., Dichgans, M., Düring, M., and Liesz, A. (2019). In vivo widefield calcium imaging of the mouse cortex for analysis of network connectivity in health and brain disease. Neuroimage *199*, 570–584.

Daigle, T.L., Madisen, L., Hage, T.A., Valley, M.T., Knoblich, U., Larsen, R.S., Takeno, M.M., Huang, L., Gu, H., Larsen, R., et al. (2018). A Suite of Transgenic Driver and Reporter Mouse Lines with Enhanced Brain-Cell-Type Targeting and Functionality. Cell *174*, 465–480.e22.

Damoiseaux, J.S., Rombouts, S.A., Barkhof, F., Scheltens, P., Stam, C.J., Smith, S.M., and Beckmann, C.F. (2006). Consistent resting-state networks across healthy subjects. Proc. Natl. Acad. Sci. USA *103*, 13848–13853.

Dana, H., Chen, T.W., Hu, A., Shields, B.C., Guo, C., Looger, L.L., Kim, D.S., and Svoboda, K. (2014). Thy1-GCaMP6 transgenic mice for neuronal population imaging in vivo. PLoS ONE *9*, e108697.

Dana, H., Mohar, B., Sun, Y., Narayan, S., Gordus, A., Hasseman, J.P., Tsegaye, G., Holt, G.T., Hu, A., Walpita, D., et al. (2016). Sensitive red protein calcium indicators for imaging neural activity. eLife *5*, 5.

Dana, H., Sun, Y., Mohar, B., Hulse, B.K., Kerlin, A.M., Hasseman, J.P., Tsegaye, G., Tsang, A., Wong, A., Patel, R., et al. (2019). High-performance calcium sensors for imaging activity in neuronal populations and microcompartments. Nat. Methods *16*, 649–657.

Das, A., and Gilbert, C.D. (1997). Distortions of visuotopic map match orientation singularities in primary visual cortex. Nature *387*, 594–598.

Denk, W., and Svoboda, K. (1997). Photon upmanship: why multiphoton imaging is more than a gimmick. Neuron *18*, 351–357.

Deverman, B.E., Pravdo, P.L., Simpson, B.P., Kumar, S.R., Chan, K.Y., Banerjee, A., Wu, W.L., Yang, B., Huber, N., Pasca, S.P., and Gradinaru, V. (2016). Cre-dependent selection yields AAV variants for widespread gene transfer to the adult brain. Nat. Biotechnol. *34*, 204–209.

Dimidschstein, J., Chen, Q., Tremblay, R., Rogers, S.L., Saldi, G.A., Guo, L., Xu, Q., Liu, R., Lu, C., Chu, J., et al. (2016). A viral strategy for targeting and manipulating interneurons across vertebrate species. Nat. Neurosci. *19*, 1743–1749.

Feng, J., Zhang, C., Lischinsky, J.E., Jing, M., Zhou, J., Wang, H., Zhang, Y., Dong, A., Wu, Z., Wu, H., et al. (2019). A Genetically Encoded Fluorescent Sensor for Rapid and Specific In Vivo Detection of Norepinephrine. Neuron *102*, 745–761.e8.

Ferezou, I., Bolea, S., and Petersen, C.C.H. (2006). Visualizing the cortical representation of whisker touch: voltage-sensitive dye imaging in freely moving mice. Neuron *50*, 617–629.

Ferezou, I., Haiss, F., Gentet, L.J., Aronoff, R., Weber, B., and Petersen, C.C.H. (2007). Spatiotemporal dynamics of cortical sensorimotor integration in behaving mice. Neuron *56*, 907–923.

Gilad, A., and Helmchen, F. (2020). Spatiotemporal refinement of signal flow through association cortex during learning. Nat. Commun. *11*, 1744.

Gribizis, A., Ge, X., Daigle, T.L., Ackman, J.B., Zeng, H., Lee, D., and Crair, M.C. (2019). Visual Cortex Gains Independence from Peripheral Drive before Eye Opening. Neuron *104*, 711–723.e3.

Grinvald, A., Lieke, E., Frostig, R.D., Gilbert, C.D., and Wiesel, T.N. (1986). Functional architecture of cortex revealed by optical imaging of intrinsic signals. Nature *324*, 361–364.

Gunaydin, L.A., Grosenick, L., Finkelstein, J.C., Kauvar, I.V., Fenno, L.E., Adhikari, A., Lammel, S., Mirzabekov, J.J., Airan, R.D., Zalocusky, K.A., et al. (2014). Natural neural projection dynamics underlying social behavior. Cell *157*, 1535–1551.

Hamodi, A.S., Martinez Sabino, A., Fitzgerald, N.D., Moschou, D., and Crair, M.C. (2020). Transverse sinus injections drive robust whole-brain expression of transgenes. eLife *9*, 1–16.

Harris, K.D., Quiroga, R.Q., Freeman, J., and Smith, S.L. (2016). Improving data quality in neuronal population recordings. Nat. Neurosci. *19*, 1165–1174.

Higley, M.J., and Sabatini, B.L. (2008). Calcium signaling in dendrites and spines: practical and functional considerations. Neuron *59*, 902–913.

Hippenmeyer, S., Vrieseling, E., Sigrist, M., Portmann, T., Laengle, C., Ladle, D.R., and Arber, S. (2005). A developmental switch in the response of DRG neurons to ETS transcription factor signaling. PLoS Biol. *3*, e159.

Hochbaum, D.R., Zhao, Y., Farhi, S.L., Klapoetke, N., Werley, C.A., Kapoor, V., Zou, P., Kralj, J.M., Maclaurin, D., Smedemark-Margulies, N., et al. (2014). All-optical electrophysiology in mammalian neurons using engineered microbial rhodopsins. Nat. Methods *11*, 825–833.

Inoue, M., Takeuchi, A., Horigane, S., Ohkura, M., Gengyo-Ando, K., Fujii, H., Kamijo, S., Takemoto-Kimura, S., Kano, M., Nakai, J., et al. (2015). Rational design of a high-affinity, fast, red calcium indicator R-CaMP2. Nat. Methods *12*, 64–70.

Jin, L., Han, Z., Platisa, J., Wooltorton, J.R., Cohen, L.B., and Pieribone, V.A. (2012). Single action potentials and subthreshold electrical events imaged in neurons with a fluorescent protein voltage probe. Neuron *75*, 779–785.

Jing, M., Zhang, P., Wang, G., Feng, J., Mesik, L., Zeng, J., Jiang, H., Wang, S., Looby, J.C., Guagliardo, N.A., et al. (2018). A genetically encoded fluorescent acetylcholine indicator for in vitro and in vivo studies. Nat. Biotechnol. *36*, 726–737.

Jüttner, J., Szabo, A., Gross-Scherf, B., Morikawa, R.K., Rompani, S.B., Hantz, P., Szikra, T., Esposti, F., Cowan, C.S., Bharioke, A., et al. (2019). Targeting neuronal and glial cell types with synthetic promoter AAVs in mice, non-human primates and humans. Nat. Neurosci. *22*, 1345–1356.

Kim, C.K., Miri, A., Leung, L.C., Berndt, A., Mourrain, P., Tank, D.W., and Burdine, R.D. (2014). Prolonged, brain-wide expression of nuclear-localized GCaMP3 for functional circuit mapping. Front. Neural Circuits *8*, 138.

Kim, T.H., Zhang, Y., Lecoq, J., Jung, J.C., Li, J., Zeng, H., Niell, C.M., and Schnitzer, M.J. (2016). Long-Term Optical Access to an Estimated One Million Neurons in the Live Mouse Cortex. Cell Rep. *17*, 3385–3394.

Kingsbury, L., Huang, S., Wang, J., Gu, K., Golshani, P., Wu, Y.E., and Hong, W. (2019). Correlated Neural Activity and Encoding of Behavior across Brains of Socially Interacting Animals. Cell *178*, 429–446.e16.

Kozberg, M.G., Ma, Y., Shaik, M.A., Kim, S.H., and Hillman, E.M.C. (2016). Rapid postnatal expansion of neural networks occurs in an environment of altered neurovascular and neurometabolic coupling. J. Neurosci. *36*, 6704–6717.

Lake, E.M.R., Ge, X., Shen, X., Herman, P., Hyder, F., Cardin, J.A., Higley, M.J., Scheinost, D., Papademetris, X., Crair, M.C., et al. (2018). Spanning spatiotemporal scales with simultaneous mesoscopic Ca2+ imaging and functional MRI. bioRxiv. https://doi.org/10.1101/464305.

Lin, M.Z., and Schnitzer, M.J. (2016). Genetically encoded indicators of neuronal activity. Nat. Neurosci. *19*, 1142–1153.

Liu, J., Whiteway, M.R., Sheikhattar, A., Butts, D.A., Babadi, B., and Kanold, P.O. (2019). Parallel Processing of Sound Dynamics across Mouse Auditory Cortex via Spatially Patterned Thalamic Inputs and Distinct Areal Intracortical Circuits. Cell Rep. *27*, 872–885.e7.

Logothetis, N.K., Pauls, J., Augath, M., Trinath, T., and Oeltermann, A. (2001). Neurophysiological investigation of the basis of the fMRI signal. Nature *412*, 150–157.

Ma, Y., Shaik, M.A., Kim, S.H., Kozberg, M.G., Thibodeaux, D.N., Zhao, H.T., Yu, H., and Hillman, E.M. (2016a). Wide-field optical mapping of neural activity and brain haemodynamics: considerations and novel approaches. Philos. Trans. R. Soc. Lond. B Biol. Sci. *371*, 20150360.

Ma, Y., Shaik, M.A., Kozberg, M.G., Kim, S.H., Portes, J.P., Timerman, D., and Hillman, E.M.C. (2016b). Resting-state hemodynamics are spatiotemporally coupled to synchronized and symmetric neural activity in excitatory neurons. Proc. Natl. Acad. Sci. USA *113*, E8463–E8471.

MacDowell, C.J., and Buschman, T.J. (2020). Low-Dimensional Spatiotemporal Dynamics Underlie Cortex-wide Neural Activity. Curr. Biol. *30*, 2665–2680.e8.

Madisen, L., Mao, T., Koch, H., Zhuo, J.M., Berenyi, A., Fujisawa, S., Hsu, Y.W., Garcia, A.J., 3rd, Gu, X., Zanella, S., et al. (2012). A toolbox of Cre-dependent optogenetic transgenic mice for light-induced activation and silencing. Nat. Neurosci. *15*, 793–802.

Madisen, L., Garner, A.R., Shimaoka, D., Chuong, A.S., Klapoetke, N.C., Li, L., van der Bourg, A., Niino, Y., Egolf, L., Monetti, C., et al. (2015). Transgenic mice for intersectional targeting of neural sensors and effectors with high specificity and performance. Neuron *85*, 942–958.

Malonek, D., and Grinvald, A. (1996). Interactions between electrical activity and cortical microcirculation revealed by imaging spectroscopy: implications for functional brain mapping. Science *272*, 551–554.

Marvin, J.S., Borghuis, B.G., Tian, L., Cichon, J., Harnett, M.T., Akerboom, J., Gordus, A., Renninger, S.L., Chen, T.W., Bargmann, C.I., et al. (2013). An optimized fluorescent probe for visualizing glutamate neurotransmission. Nat. Methods *10*, 162–170.

Marvin, J.S., Scholl, B., Wilson, D.E., Podgorski, K., Kazemipour, A., Müller, J.A., Schoch, S., Quiroz, F.J.U., Rebola, N., Bao, H., et al. (2018). Stability, affinity, and chromatic variants of the glutamate sensor iGluSnFR. Nat. Methods *15*, 936–939.

Marvin, J.S., Shimoda, Y., Magloire, V., Leite, M., Kawashima, T., Jensen, T.P., Kolb, I., Knott, E.L., Novak, O., Podgorski, K., et al. (2019). A genetically encoded fluorescent sensor for in vivo imaging of GABA. Nat. Methods *16*, 763–770.

Matsui, T., Murakami, T., and Ohki, K. (2016). Transient neuronal coactivations embedded in globally propagating waves underlie resting-state functional connectivity. Proc. Natl. Acad. Sci. USA *113*, 6556–6561.

Meng, C., Zhou, J., Papaneri, A., Peddada, T., Xu, K., and Cui, G. (2018). Spectrally Resolved Fiber Photometry for Multi-component Analysis of Brain Circuits. Neuron *98*, 707–717.e4.

Mishne, G., Coifman, R.R., Lavzin, M., and Schiller, J. (2018). Automated cellular structure extraction in biological images with applications to calcium imaging data. bioRxiv. https://doi.org/10.1101/313981.

Mohajerani, M.H., McVea, D.A., Fingas, M., and Murphy, T.H. (2010). Mirrored bilateral slow-wave cortical activity within local circuits revealed by fast bihemispheric voltage-sensitive dye imaging in anesthetized and awake mice. J. Neurosci. *30*, 3745–3751.

Montgomery, M.K., Kim, S.H., Dovas, A., Zhao, H.T., Goldberg, A.R., Xu, W., Yagielski, A.J., Cambareri, M.K., Patel, K.B., Mela, A., et al. (2020). Glioma-Induced Alterations in Neuronal Activity and Neurovascular Coupling during Disease Progression. Cell Rep. *31*, 107500.

Musall, S., Kaufman, M.T., Juavinett, A.L., Gluf, S., and Churchland, A.K. (2019). Single-trial neural dynamics are dominated by richly varied movements. Nat. Neurosci. *22*, 1677–1686.

Nakai, J., Ohkura, M., and Imoto, K. (2001). A high signal-to-noise Ca(2+) probe composed of a single green fluorescent protein. Nat. Biotechnol. *19*, 137–141.

Orsolic, I., Rio, M., Mrsic-Flogel, T.D., and Znamenskiy, P. (2019). Mesoscale cortical dynamics reflect the interaction of sensory evidence and temporal expectation during perceptual decision-making. bioRxiv. https://doi.org/10.1101/552026.

Pachitariu, M., Stringer, C., and Harris, K.D. (2018). Robustness of spike deconvolution for neuronal calcium imaging. J. Neurosci. *38*, 7976–7985.

Patriarchi, T., Cho, J.R., Merten, K., Howe, M.W., Marley, A., Xiong, W.H., Folk, R.W., Broussard, G.J., Liang, R., Jang, M.J., et al. (2018). Ultrafast neuronal imaging of dopamine dynamics with designed genetically encoded sensors. Science *360*, eaat4422.

Peron, S., Chen, T.W., and Svoboda, K. (2015). Comprehensive imaging of cortical networks. Curr. Opin. Neurobiol. *32*, 115–123.

Peters, A.J., Steinmetz, N.A., Harris, K.D., and Carandini, M. (2019). Striatal activity reflects cortical activity patterns. bioRxiv. https://doi.org/10.1101/703710.

Pisano, F., Pisanello, M., Lee, S.J., Lee, J., Maglie, E., Balena, A., Sileo, L., Spagnolo, B., Bianco, M., Hyun, M., et al. (2019). Depth-resolved fiber photometry with a single tapered optical fiber implant. Nat. Methods *16*, 1185–1192.

Puścian, A., Łęski, S., Kasprowicz, G., Winiarski, M., Borowska, J., Nikolaev, T., Boguszewski, P.M., Lipp, H.P., and Knapska, E. (2016). Eco-HAB as a fully automated and ecologically relevant assessment of social impairments in mouse models of autism. eLife *5*, 5.

Rossi, L.F., Wykes, R.C., Kullmann, D.M., and Carandini, M. (2017). Focal cortical seizures start as standing waves and propagate respecting homotopic connectivity. Nat. Commun. *8*, 217.

Rubinov, M., and Sporns, O. (2010). Complex network measures of brain connectivity: uses and interpretations. Neuroimage *52*, 1059–1069.

Rynes, M.L., Surinach, D., Linn, S., Laroque, M., Rajendran, V., Dominguez, J., Hadjistamolou, O., Navabi, Z.S., Ghanbari, L., Johnson, G.W., et al. (2020). Miniaturized head-mounted device for whole cortex mesoscale imaging in freely behaving mice. bioRxiv. https://doi.org/10.1101/2020.05.25.114892.

Saxena, S., Kinsella, I., Musall, S., Kim, S.H., Meszaros, J., Thibodeaux, D.N., Kim, C., Cunningham, J., Hillman, E.M.C., Churchland, A., and Paninski, L. (2020). Localized semi-nonnegative matrix factorization (LocaNMF) of widefield calcium imaging data. PLoS Comput. Biol. *16*, e1007791.

Schölvinck, M.L., Maier, A., Ye, F.Q., Duyn, J.H., and Leopold, D.A. (2010). Neural basis of global resting-state fMRI activity. Proc. Natl. Acad. Sci. USA *107*, 10238–10243.

Scott, B.B., Thiberge, S.Y., Guo, C., Tervo, D.G.R., Brody, C.D., Karpova, A.Y., and Tank, D.W. (2018). Imaging Cortical Dynamics in GCaMP Transgenic Rats with a Head-Mounted Widefield Macroscope. Neuron *100*, 1045–1058.e5.

Senarathna, J., Yu, H., Deng, C., Zou, A.L., Issa, J.B., Hadjiabadi, D.H., Gil, S., Wang, Q., Tyler, B.M., Thakor, N.V., and Pathak, A.P. (2019). A miniature multicontrast microscope for functional imaging in freely behaving animals. Nat. Commun. *10*, 99.

Shemesh, O.A., Linghu, C., Piatkevich, K.D., Goodwin, D., Celiker, O.T., Gritton, H.J., Romano, M.F., Gao, R., Yu, C.J., Tseng, H.A., et al. (2020). Precision Calcium Imaging of Dense Neural Populations via a Cell-Body-Targeted Calcium Indicator. Neuron *107*, 470–486.e11.

Shimaoka, D., Steinmetz, N.A., Harris, K.D., and Carandini, M. (2019). The impact of bilateral ongoing activity on evoked responses in mouse cortex. eLife *8*, 8.

Shmuel, A., Yacoub, E., Chaimow, D., Logothetis, N.K., and Ugurbil, K. (2007). Spatio-temporal point-spread function of fMRI signal in human gray matter at 7 Tesla. Neuroimage *35*, 539–552.

Silasi, G., Xiao, D., Vanni, M.P., Chen, A.C.N., and Murphy, T.H. (2016). Intact skull chronic windows for mesoscopic wide-field imaging in awake mice. J. Neurosci. Methods *267*, 141–149.

Sit, K.K., and Goard, M.J. (2020). Distributed and retinotopically asymmetric processing of coherent motion in mouse visual cortex. Nat. Commun. *11*, 3565.

Skocek, O., Nöbauer, T., Weilguny, L., Martínez Traub, F., Xia, C.N., Molodtsov, M.I., Grama, A., Yamagata, M., Aharoni, D., Cox, D.D., et al. (2018). High-speed volumetric imaging of neuronal activity in freely moving rodents. Nat. Methods *15*, 429–432.

Smith, S.L., Smith, I.T., Branco, T., and Häusser, M. (2013). Dendritic spikes enhance stimulus selectivity in cortical neurons in vivo. Nature *503*, 115–120.

Smith, G.B., Hein, B., Whitney, D.E., Fitzpatrick, D., and Kaschube, M. (2018). Distributed network interactions and their emergence in developing neocortex. Nat. Neurosci. *21*, 1600–1608.

Sofroniew, N.J., Flickinger, D., King, J., and Svoboda, K. (2016). A large field of view two-photon mesoscope with subcellular resolution for in vivo imaging. eLife *5*, 5.

Stafford, J.M., Jarrett, B.R., Miranda-Dominguez, O., Mills, B.D., Cain, N., Mihalas, S., Lahvis, G.P., Lattal, K.M., Mitchell, S.H., David, S.V., et al. (2014). Large-scale topology and the default mode network in the mouse connectome. Proc. Natl. Acad. Sci. USA *111*, 18745–18750.

Steinmetz, N.A., Buetfering, C., Lecoq, J., Lee, C.R., Peters, A.J., Jacobs, E.A.K., Coen, P., Ollerenshaw, D.R., Valley, M.T., de Vries, S.E.J., et al. (2017). Aberrant Cortical Activity in Multiple GCaMP6-Expressing Transgenic Mouse Lines. eNeuro *4*, 4.

Stern, M., Shea-Brown, E., and Witten, D. (2020). Inferring the Spiking Rate of a Population of Neurons from Wide-Field Calcium Imaging. bioRxiv. https://doi.org/10.1101/2020.02.01.930040.

Stirman, J.N., Smith, I.T., Kudenov, M.W., and Smith, S.L. (2016). Wide field-of-view, multi-region, two-photon imaging of neuronal activity in the mammalian brain. Nat. Biotechnol. *34*, 857–862.

Sun, F., Zeng, J., Jing, M., Zhou, J., Feng, J., Owen, S.F., Luo, Y., Li, F., Wang, H., Yamaguchi, T., et al. (2018). A Genetically Encoded Fluorescent Sensor Enables Rapid and Specific Detection of Dopamine in Flies, Fish, and Mice. Cell *174*, 481–496.e19.

Tang, L., and Higley, M.J. (2020). Layer 5 Circuits in V1 Differentially Control Visuomotor Behavior. Neuron *105*, 346–354.e5.

Taniguchi, H., He, M., Wu, P., Kim, S., Paik, R., Sugino, K., Kvitsiani, D., Fu, Y., Lu, J., Lin, Y., et al. (2011). A resource of Cre driver lines for genetic targeting of GABAergic neurons in cerebral cortex. Neuron *71*, 995–1013.

Tervo, D.G., Hwang, B.Y., Viswanathan, S., Gaj, T., Lavzin, M., Ritola, K.D., Lindo, S., Michael, S., Kuleshova, E., Ojala, D., et al. (2016). A Designer AAV Variant Permits Efficient Retrograde Access to Projection Neurons. Neuron *92*, 372–382.

Thompson, I.D., Kossut, M., and Blakemore, C. (1983). Development of orientation columns in cat striate cortex revealed by 2-deoxyglucose autoradiography. Nature *301*, 712–715.

Tian, L., Hires, S.A., Mao, T., Huber, D., Chiappe, M.E., Chalasani, S.H., Petreanu, L., Akerboom, J., McKinney, S.A., Schreiter, E.R., et al. (2009). Imaging neural activity in worms, flies and mice with improved GCaMP calcium indicators. Nat. Methods *6*, 875–881.

Tootell, R.B.H., Silverman, M.S., Hamilton, S.L., Switkes, E., and De Valois, R.L. (1988). Functional anatomy of macaque striate cortex. V. Spatial frequency. J. Neurosci. *8*, 1610–1624.

Tsien, J.Z., Chen, D.F., Gerber, D., Tom, C., Mercer, E.H., Anderson, D.J., Mayford, M., Kandel, E.R., and Tonegawa, S. (1996). Subregion- and cell type-restricted gene knockout in mouse brain. Cell *87*, 1317–1326.

Valley, M.T., Moore, M.G., Zhuang, J., Mesa, N., Castelli, D., Sullivan, D., Reimers, M., and Waters, J. (2020). Separation of hemodynamic signals from GCaMP fluorescence measured with wide-field imaging. J. Neurophysiol. *123*, 356–366.

Vanni, M.P., Chan, A.W., Balbi, M., Silasi, G., and Murphy, T.H. (2017). Mesoscale mapping of mouse cortex reveals frequency-dependent cycling between distinct macroscale functional modules. J. Neurosci. *37*, 7513–7533.

Villette, V., Chavarha, M., Dimov, I.K., Bradley, J., Pradhan, L., Mathieu, B., Evans, S.W., Chamberland, S., Shi, D., Yang, R., et al. (2019). Ultrafast Two-Photon Imaging of a High-Gain Voltage Indicator in Awake Behaving Mice. Cell *179*, 1590–1608.e23.

Vinck, M., Batista-Brito, R., Knoblich, U., and Cardin, J.A. (2015). Arousal and locomotion make distinct contributions to cortical activity patterns and visual encoding. Neuron *86*, 740–754.

Vogelstein, J.T., Packer, A.M., Machado, T.A., Sippy, T., Babadi, B., Yuste, R., and Paninski, L. (2010). Fast nonnegative deconvolution for spike train inference from population calcium imaging. J. Neurophysiol. *104*, 3691–3704.

Vormstein-Schneider, D., Lin, J.D., Pelkey, K.A., Chittajallu, R., Guo, B., Arias-Garcia, M.A., Allaway, K., Sakopoulos, S., Schneider, G., Stevenson, O., et al. (2020). Viral manipulation of functionally distinct interneurons in mice, non-human primates and humans. Nat. Neurosci. Published online August 17, 2020. https://doi.org/10.1038/s41593-020-0692-9.

Wang, Q., Ding, S.L., Li, Y., Royall, J., Feng, D., Lesnar, P., Graddis, N., Naeemi, M., Facer, B., Ho, A., et al. (2020a). The Allen Mouse Brain Common Coordinate Framework: A 3D Reference Atlas. Cell *181*, 936–953.e20.

Wang, T., Wu, C., Ouzounov, D.G., Gu, W., Xia, F., Kim, M., Yang, X., Warden, M.R., and Xu, C. (2020b). Quantitative analysis of 1300-nm three-photon calcium imaging in the mouse brain. eLife *9*, 9.

Wekselblatt, J.B., Flister, E.D., Piscopo, D.M., and Niell, C.M. (2016). Large-scale imaging of cortical dynamics during sensory perception and behavior. J. Neurophysiol. *115*, 2852–2866.

Worbe, Y. (2015). Neuroimaging signature of neuropsychiatric disorders. Curr. Opin. Neurol. *28*, 358–364.

Wright, P.W., Brier, L.M., Bauer, A.Q., Baxter, G.A., Kraft, A.W., Reisman, M.D., Bice, A.R., Snyder, A.Z., Lee, J.M., and Culver, J.P. (2017). Functional connectivity structure of cortical calcium dynamics in anesthetized and awake mice. PLoS ONE *12*, e0185759.

Xiao, D., Vanni, M.P., Mitelut, C.C., Chan, A.W., LeDue, J.M., Xie, Y., Chen, A.C.N., Swindale, N.V., and Murphy, T.H. (2017). Mapping cortical mesoscopic networks of single spiking cortical or sub-cortical neurons. eLife *6*, 6.

Xu, N.L., Harnett, M.T., Williams, S.R., Huber, D., O'Connor, D.H., Svoboda, K., and Magee, J.C. (2012). Nonlinear dendritic integration of sensory and motor input during an active sensing task. Nature *492*, 247–251.

Zatka-Haas, P., Steinmetz, N.A., Carandini, M., and Harris, K.D. (2019). Distinct contributions of mouse cortical areas to visual discrimination. bioRxiv. https://doi.org/10.1101/501627.